CHALMERS
UNIVERSITY OF TECHNOLOGY

An Interlaboratory Comparison of On-Wafer S-Parameter Measurements up to 1.1 THz

Citation for the original published paper (version of record):
Mubarak, F., Phung, G., Arz, U. et al (2025). An Interlaboratory Comparison of On-Wafer S-Parameter Measurements up to 1.1 THz. IEEE Transactions on Terahertz Science and Technology, In Press. http://dx.doi.org/10.1109/TTHZ.2025.3537461

An Interlaboratory Comparison of On-Wafer S-Parameter Measurements up to 1.1 THz

Faisal Mubarak, *Member, IEEE*, Gia Ngoc Phung, *Member, IEEE*, Uwe Arz, *Senior Member, IEEE*, Kamel Haddadi, *Member, IEEE*, Isabelle Roch-Jeune, Guillaume Ducournau, *Member, IEEE*, Thomas Flisgen, Ralf Doerner, *Member, IEEE*, Djamel Allal, Divya Jayasankar, *Graduate Student Member, IEEE*, Jan Stake, *Senior Member, IEEE*, Robin Schmidt, *Member, IEEE*, Gavin Fisher, Nick Ridler, *Fellow, IEEE*, Xiaobang Shang, *Senior Member, IEEE*

***Abstract*—This paper reports on an interlaboratory measurement comparison involving on-wafer S-parameter measurements from 10 GHz to 1.1 THz. Seven laboratories are involved, and each participant has measured an individual reference substrate fabricated from a high-resistivity silicon wafer in the same batch. One- and two-port co-planar waveguide (CPW) structures are designed, simulated, and fabricated. The measurements from 10 GHz to 1.1 THz, extending across six frequency bands, are conducted using different equipment in terms of vendors and specifications (e.g., probe pitch size). Despite such differences, this interlaboratory study has shown a generally good agreement between results from different participants when uncertainties are considered. The comparison with simulated reference values demonstrates agreement within 0.08 for $|S_{11}|$ and 2 dB for $|S_{21}|$ measurements of matched devices up to 1.1 THz. The measurement comparison demonstrates the need for a standardized measurement approach and, with that, a potential to achieve accurate on-wafer CPW measurements up to THz frequencies, underpinning the development of integrated circuits for such high frequencies.**

Manuscript received September 13, 2024; revised December 4, 2024.

This work was supported, in part by the EMPIR project 18SIB09 TEMMT, in part by the EPM project 23IND10 OnMicro, in part by the Dutch Ministry of Economic Affairs and Climate, in part by the Frech Renatech network, and in part by the Contrat de Plan Etat Region (CPER) WAVETECH @HdF project and Haut de-France Regional council, IEMN UHD flagship project, the IEMN CHOP platform, and France 2030-PEPR FUNTERA and SYSTERA projects, funded by ANR (Agence Nationale de la Recherche) under Grants ANR-22-PEEL-0006 and 22-PEFT-0006, French RENATECH network, the Equipex + Nanofutur (Grant IA-21-ESRE-0012). (Corresponding author: Faisal Mubarak)

Faisal Mubarak is with with the Electricity and Time Department of VSL, the National Metrology Institute of The Netherlands, Thijsseweg 11, 2629 JA Delft, The Netherlands (e-mail: fmubarak@vsl.nl).

Gia Ngoc Phung and Uwe Arz are with Physikalisch-Technische Bundesanstalt (PTB), Bundesallee 100, 38116 Braunschweig, Germany

Ralf Doerner and Thomas Flisgen are with Ferdinand-Braun-Institut gGmbH, Leibniz-Institut für Höchstfrequenztechnik, Berlin, Germany. Thomas Flisgen is also with Brandenburgische Technische Universität Cottbus- Senftenberg, 03046 Cottbus, Germany

Gavin Fisher is with Formfactor GmbH, Suss Strasse 1, Germany.

Kamel Haddadi, Isabelle Roch-Jeune, and Guillaume Ducournau are with Univ. Lille, CNRS, UMR 8520 - IEMN - Institut d'Electronique de Microélectronique et de Nanotechnologie, - Lille, France

Robin Schmidt is with Keysight Labs, Wingepark 51, Belgium.

Djamel Allal is with Laboratoire national de métrologie et d'essais (LNE), 29 Avenue Roger Hennequin, 78197 Trappes Cedex, France.

Divya Jayasankar and Jan Stake are with Terahertz and Millimetre Wave Laboratory, Department of Microtechnology and Nanoscience, Chalmers University of Technology, SE-41296 Gothenburg, Sweden. Divya Jayasankar is also with the Research Institutes of Sweden, SE-50462, Borås, Sweden.

Nick Ridler and Xiaobang Shang are with National Physical Laboratory, Teddington, TW11 0LW, UK.

***Index Terms*—Calibration, coplanar waveguides (CPW), on-wafer, S-parameter measurements, comparison, Terahertz metrology.**

I. Introduction

THE ability to sense terahertz waves in a chip-scale technology has the potential for transformative applications in sensing [1], imaging [2], and security [3]. Operational frequencies between 100 GHz and 300 GHz are expected to meet the large bandwidth requirements necessary for supporting individual user data rates of up to 100 Gbit/s envisioned for 6th generation (6G) networks [4]. All these applications require devices and integrated circuits operating at these high frequencies, with semiconductor foundries demonstrating active devices with operating frequencies exceeding 1 THz [5], [6].

The measurement infrastructure for on-wafer device characterization is critical for developing such novel devices and systems operating beyond 1 THz. Commercially available measurement equipment for Terahertz characterization is increasing steadily, with frequency extender heads for vector network analyzers (VNAs) [7], on-wafer calibration kits [8], and ground-signal-ground (GSG) probes [9] as essential components. The complexity and diversity in developing such Terahertz testbeds make it increasingly difficult to establish accurate on-wafer measurements up to the WR 1.0 band. This is also evident from the lack of traceability for on-wafer coplanar waveguide (CPW) measurements above 118 GHz, with PTB as the only NMI worldwide having CMC's for on-wafer measurements [10].

The literature review reveals increasing efforts to develop measurement techniques for on-wafer S-parameter characterization in the millimetre-wave and sub-millimetre-wave range. Williams demonstrated sub-millimetre wave transistor characterization by developing a dedicated calibration kit for the desired technology [11], an approach widely employed in on-wafer device characterization. Recent works have explored novel techniques and devices for WR 1.0 band characterization using planar goubau lines [12], [13]. A mTRL calibration up to 1 THz was demonstrated with inverted grounded-CPW devices in an InP HBT Process [14]. Likely, traceable CPW measurements on fused silica substrates [15] and membrane technology [16] have

been demonstrated for frequencies up to 110 GHz, including a comprehensive uncertainty budget for multiline-TRL (mTRL) on-wafer measurements, dominated by uncertainties arising from the reference calibration standards [15]. While [7], [17] demonstrated waveguide measurement up to WR 1.0 band and investigated the impact of repeatability and cable movements on the combined measurement uncertainty. Furthermore, other studies [18], [19] have focused on investigating the impact of drift error due to the frequency extender heads for the WR 1.0 band. Consequently, [20] recently demonstrated an on-wafer capacitor characterization up to 1.0 THz supported with uncertainty estimates.

Measurement comparisons are fundamental for the validation of such uncertainty budgets and provide increased confidence in corresponding measurements. Interlaboratory comparisons in on-wafer measurements have highlighted several considerations necessary for comparable on-wafer RF device characterization [21]–[25] such as strong dependency on the probe topology, chuck material, environmental conditions, measurement hardware, and operator skills [21].

In this effort, this work gathers five National Metrology Institutes (NMIs), two European universities, one research institute, and one leading manufacturer of millimetre-wave and THz test and measurement instrumentation to provide a comprehensive on-wafer ultra-broadband 10 GHz – 1.1 THz CPW measurement comparison. To the best of the authors' knowledge, this is the first interlaboratory comparison conducted over a frequency range spanning up to 1.1 THz. Where initial results were made available in [26], this work offers valuable and detailed insights into the expected accuracy of on-wafer measurements and EM simulation tools at high frequencies. The manuscript is organized as follows. Section II presents the design and fabrication process of the reference substrates. A wide range of calibration and validation standards are designed and fabricated to support increased calibration and verification accuracy. In addition, a parametrization study is presented to determine electrical reference values and related uncertainties. Then, Section III proceeds with describing the simulation-based approach for reference values and uncertainties evaluation of the devices used during the interlaboratory comparison. Subsequently, measurement details crucial for organizing a comparison are provided in Section IV. Finally, Section V presents the measurement campaign results and related discussions.

II. Reference Substrate Fabrication

A. Device selection and design

A set of calibration and validation CPW structures has been designed on high-resistivity silicon (HR Si) wafer to establish metrology-grade accuracy in planar S-parameter measurements. The selection of the utilized technology is based on its availability. The reference substrate consists of a low-frequency set (kit 1) including 35 devices operating from 10 GHz to 330 GHz and a high-frequency set (kit 2) with also 35 devices operating from 330 GHz to 1.1 THz, as listed in Table I. Two separate sets are designed to ensure there is one well-defined fundamental propagation mode to ensure accurate implementation of mTRL calibration. To ensure single mode of propagation, the following condition is ensured in the design of CPW devices:

$$f_{max} < \frac{c_0}{10d\sqrt{\epsilon_{r,eff}}}. \quad (1)$$

Here, f_{max} is 330 GHz for kit-1 devices, and 1100 GHz for kit-2 devices. Furthermore, d is the ground-to-ground distance of the CPW devices in kit-1 and kit-2, and c_0 is the speed of light. Finally, $\epsilon_{r,eff}$ is the effective dielectric permittivity of the substrate.

Each set includes eight transmission lines with varying lengths ranging between 610 μm and 4280 μm for kit 1 and between 120 μm and 1320 μm for kit 2. Besides transmission lines, both kits include multiple offset shorts, opens, matched loads, and fixed-distanced two-port structures embedding two one-port devices. This variety of devices allows several calibration techniques to be implemented, i.e., TRL, mTRL, unknown thru (SOLR), and 16-term methods. Furthermore, identical access structures are included in the design of every device to allow for an accurate definition of the measurement reference plane and to realize consistent and accurate measurement results.

B. Fabrication process

Two wafers have been manufactured, each with eight identical dies, including kit 1 and kit 2 structures. The microfabrication process on a 3-inch (76.2 ± 0.3 mm) high resistivity (>5000 Ω/cm) silicon (Si) wafer from Siltronix, with 275 μm (±15 μm) thickness, started with thermal oxidation of the wafer in a furnace to produce a 50 nm layer of stable silicon oxide shown in Figure 1. After deoxidation with Hydrogen Fluoride (HF), a 50 nm dry thermal oxide (TOX) was grown by APCVD (atmospheric pressure chemical vapour deposition) at 1100 °C. Then, a resist bilayer was spin-coated and patterned using e-beam lithography with a Nano Maker EBPG-5000 Plus (Vistec^{TM}) for the definition of thin-layer resistors. Following exposure, the resist was developed to remove the exposed areas and create the desired pattern. Subsequently, a 23 nm Titanium (Ti) layer (measured mean value) was evaporated, and the lift-off process was performed to form the set of resistors. Afterward, spin-coating, alignment, and e-beam lithography of a new resist bilayer were conducted to define the CPW structures. The resist was again developed to ensure clean patterning before metal deposition. Finally, a 25 nm adhesion Ti layer and a Gold (Au) layer were deposited and lifted off (resulting in a Ti/Au average thickness of 485 nm). Eight identical reference dies were fabricated on the same wafer. In Figure Figure 2, Scanning Electron Microscope (SEM) images of the reference substrate are shown.

C. Parameterization and characterization

Relevant parameters affecting the electrical properties of the reference structures are identified and measured to

TABLE I: Overview of CPW devices in kit 1 and kit 2

Structure	Physical length (μm)	Ground type	Structures in each kit	Purpose
Thru	kit 1: 500 kit 2: 120	NA	3	system calibration
Lines	kit 1: 610 - 4280 kit 2: 155 - 1320	NA	8	system calibration
Short-Short	kit 1: 944 kit 2: 340	Ground Connected & Ground Open	1 & 1	system calibration
Mismatched line	kit 1: 1200, 2940 kit 2: 342, 894	NA	2	Interlaboratory comparison
Attenuator	kit 1: 944 kit 2: 340	NA	1	Interlaboratory comparison
Filter	kit 1: 944 kit 2: 340	NA	1	Interlaboratory comparison
Short-Short	kit 1: 0, 1044, 1264, 1444 kit 2: 0, 380, 450, 520	GC & GO	4 & 4	Interlaboratory comparison
Open-Open	kit 1: 944 kit 2: 340	Ground Connected & Ground Open	1 & 1	Probe crosstalk
Load-Load	kit 1: 944 kit 2: 340	Ground Connected & Ground Open	1 & 1	Probe crosstalk
Load-Open	kit 1: 944 kit 2: 340	Ground Connected & Ground Open	1 & 1	Probe crosstalk
Open-Short	kit 1: 944 kit 2: 340	Ground Connected & Ground Open	1 & 1	Probe crosstalk
Load-Short	kit 1: 944 kit 2: 340	Ground Connected & Ground Open	1 & 1	Probe crosstalk

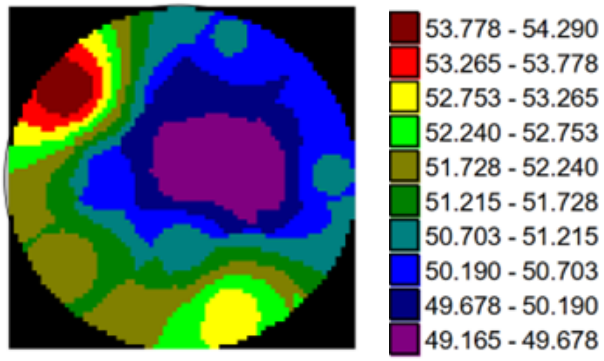

Fig. 1: A 2D mapping of the silicon oxide thickness with an average of 53 nm and 51 nm for both wafers, respectively.

assess high-frequency behavior through 3D electromagnetic (EM) simulations, as outlined Section III. First, before the fabrication of the reference substrate, the sheet resistance was calibrated on a 0.25-inch gallium arsenide (GaAs) wafer to achieve an experimental value of 50.5 Ω. Then, after the fabrication of the reference kits, a mechanical profilometer was used to measure Ti and Ti/Au thicknesses corresponding to the resistive and conductive layers, respectively. The sheet resistance was measured using a non-contact resistivity measurement technique. A Tescan Mira XMU scanning electron microscope (SEM) was used to measure the critical dimensional parameters of CPW structures. For each of the eight dies, 15 parameters of CPW devices from kit 1 and kit 2 have been characterised. The images were processed offline to limit electron charging by the SEM, as shown in Figure 2. The uncertainty for each parameter across eight dies is determined, as shown in Table II for the thru structure. The values obtained for the CPW dimensions were taken into account in the uncertainty estimation.

TABLE II: The nominal values and uncertainties of thru device parameters from kit 1 and kit 2.

Parameter		kit 1 value	kit 2 value	Uncertainty
Width (μm)	A, A'	100	29.2	2-4 %
	D, D'	54	17.4	2-4 %
	G, G'	100	29.2	2-4 %
	C	25	9.0	2-4 %
	F	11	3.5	3-4 %
	I	25	9.0	2-4 %
Length (μm)	L	500	120	2 %
Spacing (μm)	B, B'	15.96	6.3	3-5 %
	E, E'	8	2.6	3-5 %
	H, H'	15.96	6.3	3-5 %
Substrate	ϵ_r	11.80	11.80	3 %
	T_{Si} (μm)	275	275	5.5 %
Thickness (μm)	T_{gold}	0.525	0.525	4 %

III. Reference Substrate Evaluation

This section outlines the method for evaluating the reference values and uncertainties corresponding to the devices used for the interlaboratory comparison. First, EM simulations in CST Studio Suite® are employed to evaluate the S-parameters corresponding to each CPW device from kit 1 and kit 2, as listed in Table I. However, the fabrication process tolerances, as shown in Table II, introduce variations in the S-parameters of the CPW devices. The dimensional and material parameter variations resulting from the fabrication process tolerances are propagated via EM simulations using the method proposed in [27] to quantify the S-parameter uncertainty.

The second step involves evaluating the reference value and combined uncertainty for each device resulting after the calibration. The fabrication process uncertainty of every

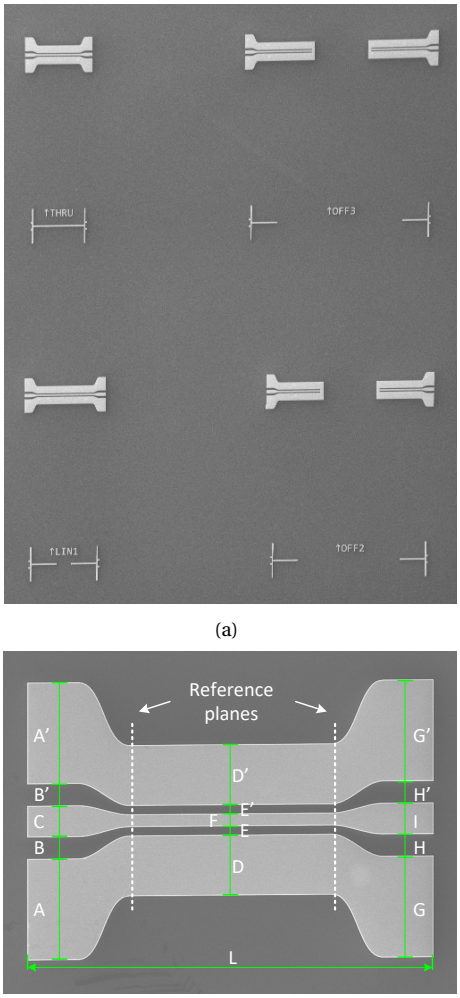

(a)

(b)

Fig. 2: SEM image of (a) reference substrate showing a section including four CPW structures from kit 1 and (b) the thru standard from kit 2 including various device parameters measured for uncertainty evaluation.

calibration device contributes to the combined uncertainty corresponding to the devices used in the comparison. For this, Monte-Carlo simulations are employed to evaluate the combined uncertainty of each comparison device.

A. Simulation approach

To calibrate each CPW device and determine the combined uncertainty, EM simulations are employed to acquire the necessary data for all CPW devices embedded in kit-1 and kit-2. First, the so-called uncorrected (RAW) data is acquired with EM simulation of all structures, including advanced probe models designed for kit-1 and kit-2 operation. Dedicated probe models are designed for kit-1 and kit-2 structure simulations. In Figure 3(a), for brevity, only the probe model for kit-1 is shown. The probe is positioned to emulate realistic measurement conditions to the device, as it would during an actual on-wafer measurement.

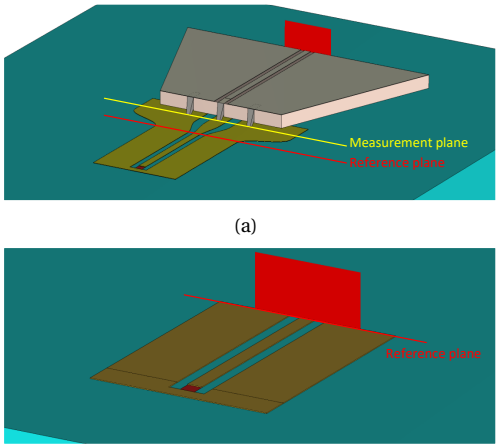

(a)

(b)

Fig. 3: (a) Acquisition of EM simulation-based raw data for the calibration standards. (b) Acquisition of EM simulation-based reference data for the calibration standards at the reference plane position.

TABLE III: A summary of CST Studio Suite® simulation settings.

Parameter	Value
Background	normal (vacuum)
Boundaries	open boundary
Solver	frequency domain
Solver order	3rd order
Mesh type	hexahedral mesh
Mesh resolution	$> 1{\cdot}10^{6}$ cells
Accuracy	$1{\cdot}10^{-4}$
Excitation	waveguide ports

Different combinations of parameter variations, resulting from the fabrication process tolerances shown in Table II, are then propagated through these EM simulations to determine a configuration that produces the maximum deviation from nominal S-parameter results. The S-parameter deviation from the nominal values of a kit-1 offset-short structure is shown in Figure 4 for assorted combinations of parameter variations. The configuration with the most significant offset in S-parameters, denoted with the combination(max), is subsequently used to acquire the uncorrected S-parameter and uncertainty of all devices in kit-1 and kit-2. In Table III, a summary of CST Studio Suite® simulation settings is shown. It was not possible to measure all dimensions of every structure throughout the eight calibration dies manufactured for the comparison participants, and only 15 selected dimensions on each die were measured. Hence, due to the lack of information, the configuration with the most significant offset is used to estimate device uncertainty instead of the most probable combination.

B. Reference S-parameter & Uncertainty

Using the uncorrected S-parameter results acquired in the previous section, the corrected S-parameter values for all devices are determined using the Multiline-Thru-

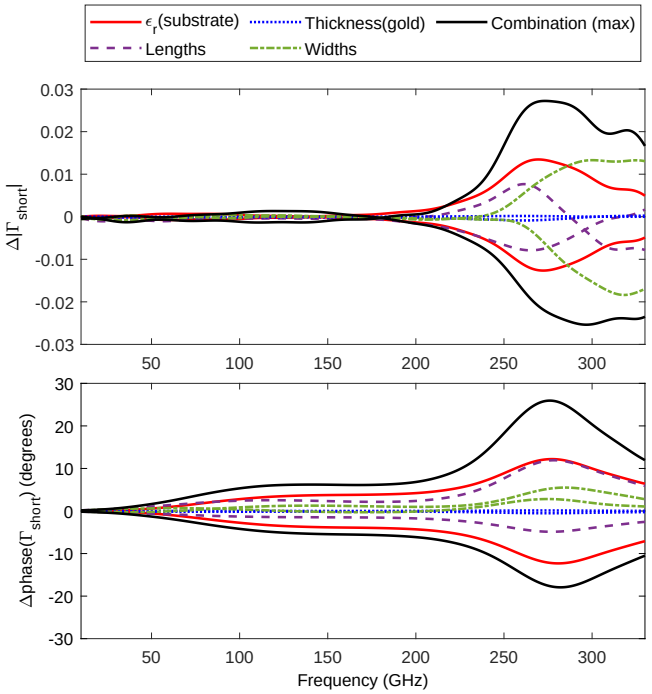

Fig. 4: S-parameter variations for kit-1 short structure estimated with EM simulations. The S-parameter results acquired for the various parameter settings are normalized to the S-parameter results acquired for nominal parameter values.

Reflect-Line (mTRL) calibration method. For this, first, S-parameters of only the TRL calibration devices are acquired with EM simulation at the pre-defined reference plan position, as shown in Figure 3(b). Once the reference data of the calibration devices is acquired, the uncorrected data of all devices is corrected using the TRL calibration method. Simultaneously, the combined uncertainty of each device is estimated using the Monte-Carlo approach, as shown in Figure 5. In total, 1000 samples were used for each frequency point during the Monte-Carlo simulations, which were found sufficient during the Monte-Carlo verification experiment.

The corrected simulation results, referred to as reference values, for all comparison devices, are shown in Figure 6. The blue lines depict the reference value for each device, and the corresponding uncertainty is identified with the blue-colored region. The reference value uncertainty accounts for the fabrication process uncertainty of every calibration device used for correcting the comparison device S-parameters and the probe crosstalk uncertainty detailed in Section V-A. The uncertainty of the EM simulation itself is not accounted for in this uncertainty analysis, which can typically range up to 5 % or even higher for 3D structures, as it depends on several factors, i.e., solver type, mesh quality, material properties, and frequency considerations [28]. The simulation accuracy most likely degrades with increasing frequencies due to the lack of material accuracy at higher frequencies.

IV. Measurement Details

This section outlines the interlaboratory measurement comparison details for on-wafer S-parameter measurements up to 1.1 THz. The comparison covers an extensive frequency range, including six frequency bands collectively supported by all participants. The measurement comparison participants and details of the various measurement systems are provided in section IV-A. Detailed information on the comparison devices and the corresponding measurement parameters are provided in section IV-B. The most critical part of a measurement comparison is the reference value corresponding to each parameter being compared. Description of the reference value and uncertainty corresponding to the comparison devices are provided in section IV-C. The reference substrate is designed to support mTRL calibration to support the extensive frequency range of the comparison, with more information provided in section IV-D. Finally, section IV-E summarizes uncertainty sources involved in on-wafer measurements and details of the combined measurement uncertainty supported by PTB measurements.

A. Participants

Each participant is provided with an individual reference substrate due to the destructive nature of on-wafer measurements. Each reference substrate includes two kits, with kit-1 supporting measurements in the coaxial frequency range up to 110 GHz, the WR6, WR5, and WR3 waveguide bands. Whereas kit-2 supports measurements in the WR2, WR1.5, and WR1 waveguide bands. Section II provides detailed information on the reference substrate design and fabrication. The measurements for kit 1 range from 10 GHz to 330 GHz and are conducted by the National Physical Laboratory (NPL), Physikalisch-Technische Bundesanstalt (PTB), Ferdinand-Braun-Institut (FBH), and Keysight Technologies® (Keysight). Whereas measurements for kit 2 range from 330 GHz to 1.1 THz and are conducted by the University of Lille (Lille), Chalmers University of Technology (Chalmers), and Form Factor®. Table IV shows

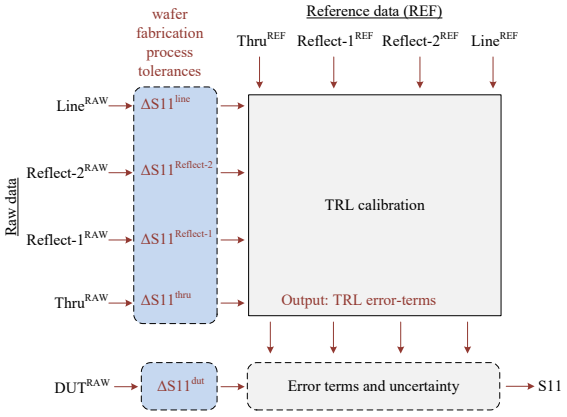

Fig. 5: Monte-Carlo simulation setup used to propagate wafer fabrication tolerances for mTRL calibration.

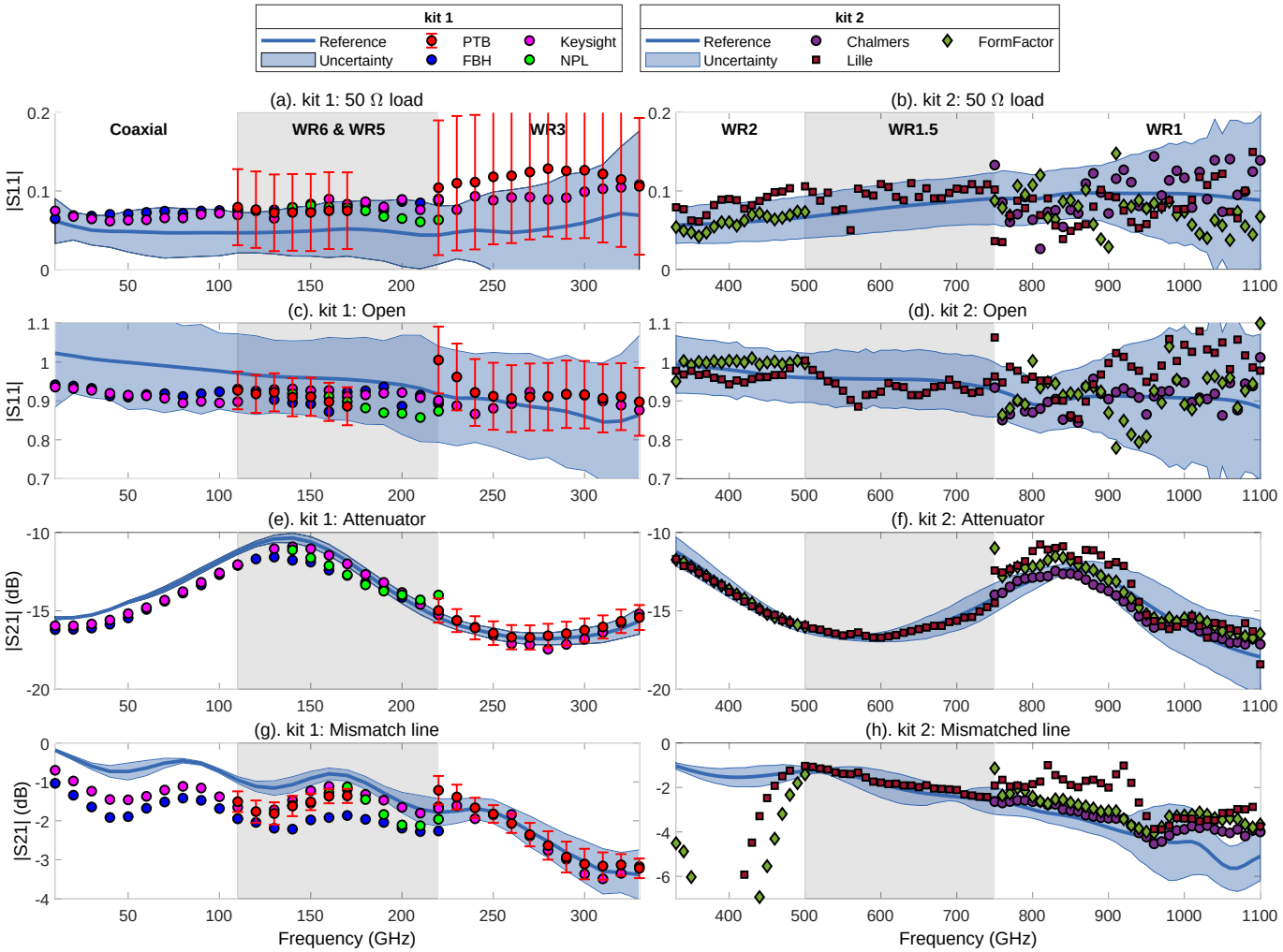

Fig. 6: Comparison device reference values determined by the median of the measurement results for kit 1 and kit 2. Data depicted with round markers correspond to kit 1 devices, and data using square markers belong to kit 2 devices.

an overview of the measurement systems used by the participants.

B. Comparison devices

The selection of the comparison devices is such to provide coverage across the match and highly mismatched loading conditions for the reflection coefficient (S_{11}) parameter. Therefore, two one-port devices are selected to compare the S_{11} parameter: a matched load and a highly mismatched open device. For the transmission (S_{21}) parameter, the selection of the devices enables comparison across a broad transmission parameter dynamic range. Hence, a mismatched transmission line and an attenuator device are selected. Both the magnitude and phase parameters are considered in the comparison. All comparison devices have different electrical characteristics compared to calibration standards used for the mTRL calibration employed to correct the data and, therefore, are appropriate for verification and comparison. In Table V, an overview of the comparison devices and the corresponding parameter is provided.

C. Comparison reference value

The interpretation of the comparison reference value is preferably based on traceable measurement results acquired during the comparison using methods as outlined in [29]. However, as only PTB provided the uncertainty estimates corresponding to their measurements, it is not possible to determine the reference values for the comparison devices using participant measurement results. Hence, the reference value and the corresponding uncertainty for each comparison device shown in Table V are determined with EM simulations using methods outlined in section III.

D. Calibration method

The mTRL method is widely regarded as one of the most accurate on-wafer calibration techniques [30]. For instance, in the inter-laboratory study [31] performed by three laboratories in the 140 to 220 GHz frequency band with different calibration approaches (Short-Open-Load-Thru (SOLT), on-wafer mTRL and off-wafer TRL) reliable results could only be obtained by on-wafer mTRL calibration. On-wafer mTRL currently represents the best choice for calibrations

TABLE IV: Details of the measurement systems used by the participants.

Frequency band	Laboratory	VNA	Probe (pitch)	Frequency extender	Chuck	Probing system
coaxial	Keysight	Keysight PNA-X 5247B	Infinity (100 μm)	N5295A (M4)	Ceramic	Form Factor CMX300
	FBH	Anritsu MS4647B	T220A (50 μm)	Anritsu MA25400A	Ceramic	Cascade PA200
WR6 WR5	Keysight	Keysight PNA-X N5292A	DMPI (50 μm)	VDI Mini	Ceramic	Form Factor CMX300
	FBH	Anritsu MS4647B	T220A (50 μm)	Anritsu MA25400A	Ceramic	Cascade PA200
	NPL	Keysight PNA-X N5247B	GGB (75 μm)	VDI	Ceramic	MPI TS-150
	PTB	Anritsu VectorStar	GGB (50 μm)	VDI	Ceramic	MPI TS-150
WR3	Keysight	Keysight PNA-X N5292A	DMPI (50 μm)	VDI Mini	Ceramic	Form Factor CMX300
	PTB	Anritsu VectorStar	GGB (50 μm)	VDI	Ceramic	MPI TS-150
WR2	LILLE	Rohde & Schwarz ZVA24	T-Wave (25 μm)	Rohde & Schwarz Z500	Absorber	Formfactor EPS200
	FormFactor	Keysight PNA	T-Wave (25 μm)	VDI	Ceramic	FormFactor Summit 200
WR1.5	LILLE	Rohde & Schwarz ZVA24	T-Wave (25 μm)	VDI VNAX	Absorber	Formfactor EPS200
WR1	LILLE	Rohde & Schwarz ZVA24	T-Wave (25 μm)	Rohde & Schwarz ZC1100	Absorber	Formfactor EPS200
	Chalmers	Keysight PNA-X N5242A	T-Wave (25 μm)	VDI	Absorber	MPI TS-150
	FormFactor	Keysight PNA	T-Wave (25 μm)	VDI	Ceramic	FormFactor Summit 200

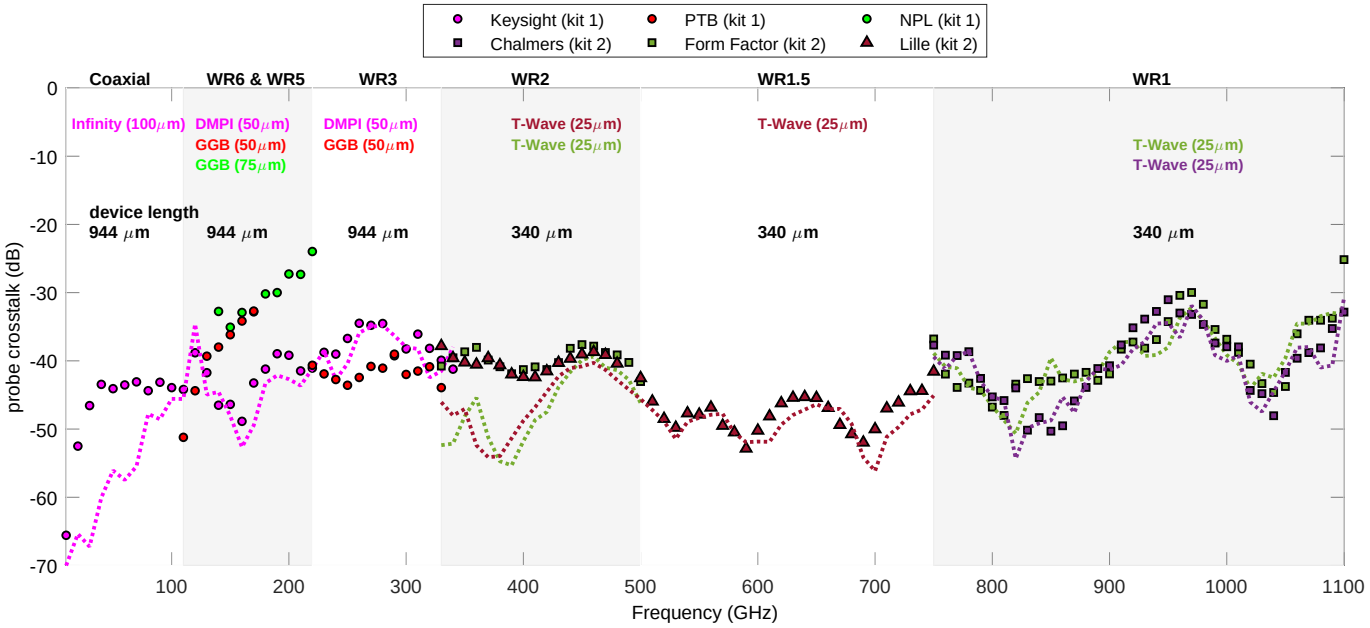

Fig. 7: Probe crosstalk measured with two-port devices comprising of two one-port structures as shown in Table I, i.e. Load-Open (LO), Open-Short (OS), and Load-Short (LS). Data depicted with markers are estimated using the set of structures without a common ground plane, and data shown with dotted lines are for structures with a common ground plane.

TABLE V: An overview of the comparison devices and parameters.

Device	Parameter	Unit
Matched load (1-port)	S_{11}	Linear magnitude
Open (1-port)	S_{11}	Linear magnitude
Attenuator (2-port)	S_{21}	Log magnitude (dB)
Mismatched line (2-port)	S_{21}	Log magnitude (dB)
Mismatched line (2-port)	S_{21}	Phase (degrees)

of millimetre-wave and THz VNA measurement systems. Hence, the mTRL method is employed in the measurement comparison campaign. Participants were allowed to use a different combination of eight transmission lines for the mTRL calibration of their system, as shown in Table I.

It is common practice to verify the quality of the calibration using the measured complex propagation constant or the measured complex effective relative dielectric constant of the transmission lines. Higher-order modes of propagation and probe cross-talk may be observable, allowing us to relate these irregularities to the discrepancies observed in calibration results. Unfortunately, we did not collect this data during the interlaboratory comparison. In addition, the participants calibrated their measurements based on different implementations of the mTRL algorithm [32], [33], [34]. A more particular case is Keysight, whose results were calibrated based on an optimal mTRL with additional probe misplacement compensation as realized in [35].

All measurement results presented in this interlaboratory comparison correspond to a reference impedance defined by the characteristic impedance of the transmission line standards. Therefore, the characteristic impedance Z_0 was not computed, and no renormalization to 50 Ω was applied to the corrected results. Consequently, any discrepancies related to the reference impedance will most likely arise

from the variations observed between different calibration substrates.

E. Measurement uncertainty

Several types of uncertainty sources generally stem from external and internal disturbances in on-wafer measurements. Internal effects originate from the transmission lines, i.e., radiation and dispersion effects. To incorporate the internal disturbances from radiation or dispersion effects, the uncertainty estimation has been revised to implement the new improved CPW model [36]. External effects, on the other hand, stem from disturbances such as e.g. the influence of microwave probes, the impact of the neighbourhood, propagation of parasitic modes (e.g. surface waves and parallel plate modes) due to the measurement boundary condition and radiation effects from the probes. Due to the complexity of the nature of these effects, a series of studies has been performed to allow for a better understanding of these effects [37]–[39].

With the benefit of hindsight, the layout of both kits has been optimized to mitigate the influence of these uncertainty sources as much as possible. Thus, the remaining uncertainty sources stem from the VNA, cables, and frequency extenders which can still be estimated according to the guide for VNA-based measurement methods [40].

The uncertainties corresponding to the PTB measurements are calculated according to the comprehensive measurement model and the procedure described in [15], making use of the improved CPW model of [36]. The PTB uncertainty budget takes into account instrumentation errors such as VNA noise, linearity, drift, cable stability, contact repeatability, uncertainties from crosstalk between the measurement ports, and CPW calibration standard uncertainties. Due to differences in the measurement equipment used by the participants, these uncertainties are valid for the PTB measurements only, which were performed in D-band and J-band, respectively. Table VI shows an overview of the uncertainty sources supported by the PTB and simulation uncertainty analysis.

Furthermore, participants did not provide details corresponding to the exact combination of transmission lines used for the implementation of their mTRL calibration. Hence, no fixed and optimum combination of transmission lines was set, and additional measurement errors may have been introduced if delays between each pair of transmission lines had not been well chosen by the participants. For example, PTB used all eight transmission lines to implement the mTRL calibration.

TABLE VI: An overview of uncertainty sources accounted for by the PTB measurements and simulated reference values.

Uncertainty source	PTB measurements	Simulated values
calibration standards	yes	yes
system noise	yes	no
system linearity	yes	no
system drift	yes	no
cable stability	yes	no
cross-talk	yes	yes
contact repeatability	yes	no

V. Measurement results and discussion

This section presents the interlaboratory comparison measurement results for kit 1 and 2 devices for frequencies up to 1.1 THz. The measurement results submitted by all participants for the comparison devices are shown in Figure 6. Here, measurement results for kit 1 and kit 2 devices are denoted with round and square markers, respectively. The results are collected across three frequency bands with kit 1 devices measured from 10 GHz up to 330 GHz. While measurement results for kit 2 devices range from 330 GHz to 1.1 THz and are accumulated across three waveguide bands. In Table IV, participant details are provided for each frequency band.

Comparison results are analyzed by calculating the difference between the measurement, and the simulation-based reference value for each participant, as shown in Figure 8 and Figure 9. First, the probe crosstalk measurements are evaluated, and then the measurement results for each frequency band are separately discussed.

A. Results for probe crosstalk

The probe crosstalk is estimated by taking the maximum value acquired for the $|S_{21}|$ and $|S_{12}|$ measurement results acquired for devices comprising of two one-port equidistant structures as listed in Table I. This includes all devices identified with 'probe crosstalk', i.e., Load-Open (LO), Open-Short (OS), and Load-Short (LS). The devices are designed to maintain a constant distance between the probes; for kit-1, the two one-port devices are distanced by 944 μm, and for kit-2, the distance is 340 μm. Furthermore, each set of devices is manufactured two-fold: a set with both devices sharing a common ground and a set with both devices having an isolated ground. The selection of devices is such to offer a wide range of loading conditions to the probes and allows the compilation of crosstalk performance for a variety of different probe types, as shown in Table IV.

We estimate probe crosstalk for the set of devices with a common ground plane and the set of devices without a common ground plane separately. This approach includes sensitivity to the load impedance, as eight devices are used for probe crosstalk analysis using the following:

$$\text{probe crosstalk} = \max_{(x\neq y\in 1,2)} \big(|S_{xy}(SS)|, |S_{xy}(OO)|, |S_{xy}(LL)|, |S_{xy}(LO)|, |S_{xy}(OS)|, |S_{xy}(LS)|\big). \quad (2)$$

Here, subscript denotes the combination of devices fabricated, i.e., SS denotes Short-Short, and LO denotes Load-Open pair.

The probe crosstalk results are shown in Figure 7. First, the probe crosstalk values for the coaxial frequency range are evaluated. Here, only Keysight could provide measurement data, including crosstalk information. Here, superior crosstalk performance is visible when comparing results acquired at 10 GHz with those collected at 110 GHz, an intuitive attribute. The more interesting attribute is the difference between the crosstalk performance for structures

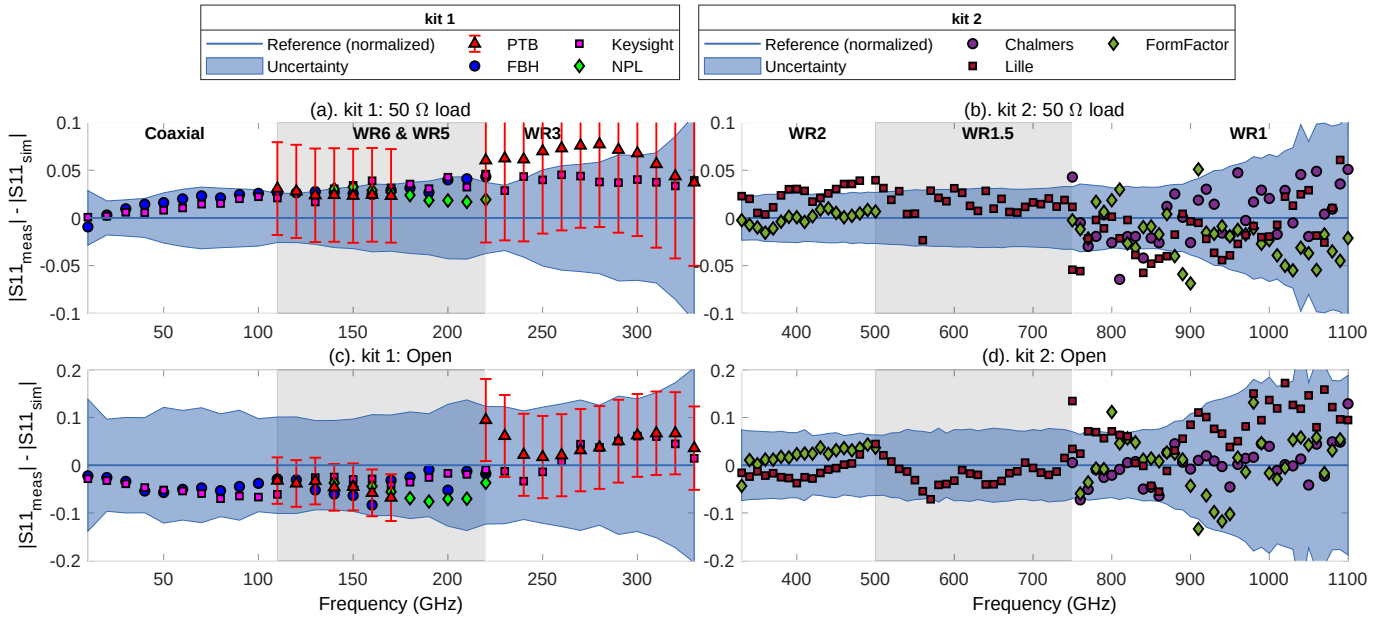

Fig. 8: Comparison results for reflection coefficient measurements of one-port load and open from kit 1 and kit 2.

with an isolated ground shown in markers and those devices with a common ground depicted with dotted lines in Figure 7. Up to 110 GHz, devices with isolated ground provide better crosstalk performance.

In the WR5 frequency range, three participants submitted crosstalk data. Here, two participants (PTB and NPL) used GGB (by GGB Industries Inc.) probes, and Keysight used DMPI (by Dominion MicroProbes Inc.) probes. It is evident from Figure 7 that the DMPI probes show better crosstalk performance as compared with GGB probes. In the WR5 frequency band, the GGB probes exhibit crosstalk degradation proportional to the frequency, a finding confirmed by data provided by NPL and PTB. The WR3 frequency range shows comparable crosstalk performance for the DMPI and GGB probes, comparable to the values noted in the WR2 band. Also, no significant difference in crosstalk performance is evident for the devices with and without a shared ground.

The crosstalk data for the WR2, WR1.5, and WR1 bands is acquired using T-Wave probes (by FormFactor Inc.), collectively submitted by three participants (Lille, Chalmers, and FormFactor). The WR2 band shows slightly larger crosstalk values as compared to those acquired for the WR1.5 band. It is interesting to see notable 5-10 dB lower crosstalk values in the WR1.5 band when using an absorber, and there is no clear reason for this, as similar probes are also used in the other frequency bands. Also, devices with common ground show a better crosstalk performance in the WR2 band, while no notable difference is evident for the WR1.5 and WR1 bands.

The crosstalk measurement results acquired up to 1.1 THz, covering six frequency bands, do not show abrupt shifts when transitioning between the different frequency bands. It is evident from Figure 7 that crosstalk performance does not show noteworthy degradation proportional to the frequency, a key attribute of this study. Also, no significant difference in crosstalk performance is noted for devices with and without a common ground. Finally, the crosstalk values shown in Figure 7 do not indicate the crosstalk performance seen in typical commercial nanoscale technologies, i.e., CMOS and SiGe BiCMOS. The limitations in the available area in such technologies will most likely not allow usage of probe distances as in this interlaboratory comparison.

B. Results for the coaxial frequency range

Figure 6(a),(c),(e), and (g) show the measurement and reference values for the kit-1 comparison devices. Here, two participants, Keysight and FBH, provided their measurement results acquired with test beds with frequency extenders as the most notable difference.

When evaluating the reflection coefficient parameters for the matched load and open device shown in Figure 8, a good agreement is observed as the differences between measurement and reference values are smaller than the reference value uncertainty up to 110 GHz.

However, the transmission parameter magnitude results shown in Figure 9 illustrate a considerable systematic difference between the measurement and reference values, which is larger than the reference value uncertainty. When evaluating the transmission parameter values for mismatched transmission line shown in Figure 6(g), the measurements results already show around 1 dB loss at 10 GHz, whereas the simulation results at 10 GHz are closer to 0.2 dB which seems more intuitive. The magnitude of the transmission parameters in the coaxial band seems to be influenced by the aging of the structures on the substrate, which might have caused considerable differences. Furthermore, measurement results for the transmission parameter phase are found to be in good agreement with the reference values.

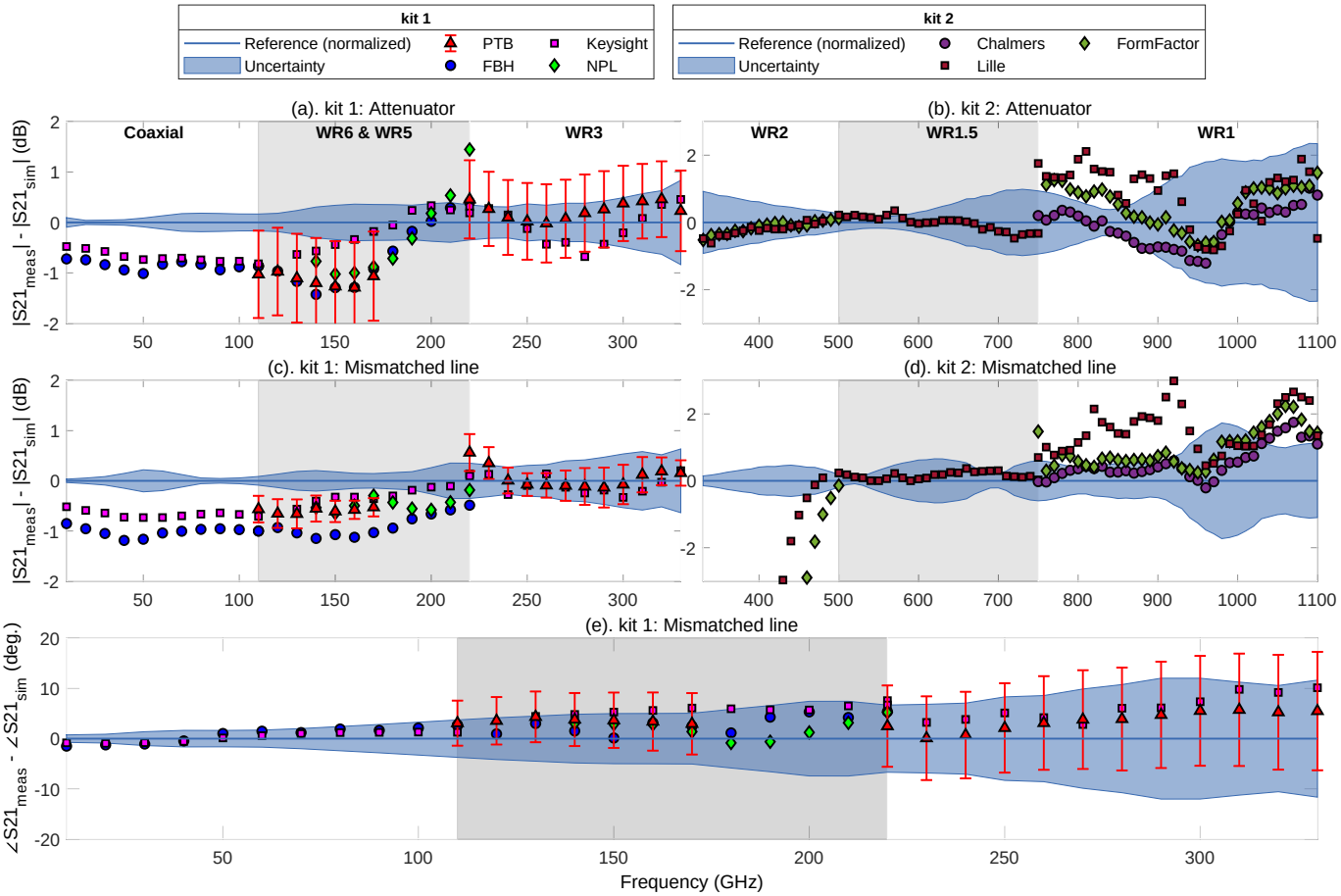

Fig. 9: Comparison results for transmission coefficient measurements of two-port attenuator and mismatched line from kit 1 and kit 2.

Finally, no notable difference is observed between the measurement results submitted by the two participants resulting from the differences in the measurement systems listed in Table IV.

C. Results for the WR6 & WR5 frequency range

For the WR6 and WR5 frequency bands, four participants provided their measurement results. Here, FBH and Keysight provided data for the entire frequency range, while PTB submitted data from 110 GHz to 170 GHz, and NPL provided data ranging from 130 GHz to 220 GHz. Furthermore, PTB is the only participant who submitted measurement results supported with uncertainty evaluation. All four participants collected the measurement data using a ceramic chuck, while different combinations of probes and frequency extender units were used. Analyzing comparison results from Figure 8 and Figure 9, no notable differences are observed as a result of different hardware usage.

When evaluating the reflection coefficient parameter values for the matched load and open device shown in Figure 8, like for the coaxial band, also here a good agreement is observed as the differences between measurement and reference values. Furthermore, PTB measurement uncertainties also show a strong agreement with the simulation values.

However, like for the coaxial band, the transmission parameter magnitude results shown in Figure 9 illustrate large differences between the measurement and reference values, larger than the reference value uncertainty for most of the WR5 frequency band. Also here, the transmission parameters in the WR6 and WR5 bands seem to be influenced by the aging of the structures on the substrate. Measurement uncertainties of PTB for the transmission parameter magnitude also seem similar to those evaluated for the reference values. However, analyzing the differences observed between the four participants, it seems that substrate aging may have a considerable impact on the transmission parameter magnitude in the coaxial and WR5 bands. Meanwhile, measurement results for the transmission parameter phase agree with the reference values.

D. Results for the WR3 frequency range

Two participants, Keysight and PTB, contributed with measurement data in the WR3 band. Here, the most notable difference in the employed measurement systems is the used probe, where Keysight used DMPI probes, and PTB used the GGB probes.

First, the reflection coefficient results are analyzed, as shown in Figure 8(a)-(c). The Keysight results for the matched load are in better agreement with the reference values. It is worth mentioning the difference between all measurement and reference values is still smaller than the reference value uncertainties. Here, PTB measurements are supported by a detailed uncertainty evaluation and are of similar order to reference value uncertainties.

Unlike results for the coaxial, WR6, and WR5 bands, the transmission parameter magnitude results for the WR3 band shown in Figure 9(a)-(c) are in good agreement with the reference values, as the differences for all measurement results are smaller than the reference value uncertainties. It seems the transmission parameters of the structures on the substrate are less sensitive for frequencies exceeding 220 GHz. Finally, measurement results for the transmission parameter phase are also in strong agreement with the reference values.

E. Results for the WR2 frequency range

Figure 6(b),(d),(f), and (g) show the measurement and reference values for the kit-2 comparison devices. Two participants, LILLE and FormFactor, contributed with measurement data in the WR2 band. Here, the most notable difference in the operated measurement systems is the chuck, where LILLE used an absorber, and FormFactor used a ceramic chuck.

The reflection coefficient measurement results for the matched load and open device shown in Figure 8(b)-(d) reveal a good agreement, as the differences between measurement and reference values are smaller than the reference value uncertainty throughout the WR2 band. However, for LILLE at some frequencies, the matched load results are outside the reference value uncertainty.

The transmission parameter magnitude results for the attenuator device are shown in Figure 9(b) and are in good agreement with the reference values, as the differences for all measurement results are smaller than the reference value uncertainties. However, measurement results for the mismatched line shown in Figure 9(d) depict a considerable difference between the measurement and reference values, larger than the reference value uncertainty. When evaluating the results of both participants for the mismatched line shown in Figure 6(h), a significant discrepancy is noted throughout the WR2 band, which is not observed for the attenuator device. A possible cause for this might be the design of the mismatched line itself, as measurement results for other verification devices seem to be correct. Another possible cause for this might have been the selection of the transmission lines for implementing the mTRL calibration, and errors might result if the phase delay between each pair of lines is not well chosen by the participants.

F. Results for the WR1.5 frequency range

In the WR1.5 band, only LILLE submitted measurement data. The reflection coefficient measurement results for the matched load and open device shown in Figure 8(b)-(d) reveal a satisfactory agreement, as the differences between measurement and reference values are smaller than the reference value uncertainty throughout the WR2 band, excluding few outliers.

Unlike for the WR2 band, here, the transmission parameter magnitude results for the attenuator and mismatched line shown in Figure 9(b)-(d) are in adequate agreement with the reference values, as the differences for all measurement results are smaller than the reference value uncertainties.

G. Results for the WR1 frequency range

Three participants, LILLE, Chalmers, and FormFactor, contributed with measurement data in the WR1 band. Here, the most notable difference in the operated measurement systems is the chuck, where LILLE and Chalmers used an absorber, and FormFactor used a ceramic chuck.

The reflection coefficient measurement results for the matched load and open device shown in Figure 8(b)-(d) reveal a reasonable agreement, as the differences between measurement and reference values are smaller than the reference value uncertainty for a majority of the measurement values throughout the WR1 band. However, measurement values shown in Figure 6(b)-(d) indicate large frequency-dependent variation observed for all participant data. However, reference value uncertainties appearing proportional to frequency demonstrate a strong increment in the WR1 band and support the increased variance observable in the measurement results.

The transmission parameter magnitude results for the attenuator device are shown in Figure 9(b) and are in good agreement with the reference values for Chalmers and FormFactor data, as the differences for the majority of the measurement results are smaller than the reference value uncertainties. However, measurement results for Lille show larger differences, especially at the start of the WR1 band. The transmission parameter results by Lille seem to show a strong variation around 950 GHz and might be caused by a poor probe contact during the through or line measurements for implementing the mTRL calibration in WR1 band. The mismatched line results shown in Figure 9(d) depict a considerable difference between the measurement and reference values for Lille as well. However, reasonable agreement is observable for Chalmers and FormFactor data. Measurement results beyond 950 GHz seem to have a good agreement between the participants and depict less loss compared with simulation results. It seems likely the simulated reference values for the mismatched line exceeding 950 GHz are accounting for too much material loss than reality. Furthermore, the reference value uncertainties decline after 1 THz and cause the measurement agreement to exceed the uncertainty region. Overall, the WR1 band shows a reasonable agreement up to 1.1 THz.

H. General remarks

The comparison results for the reflection coefficient magnitude of one-port devices are shown in Figure 6 and

Figure 8. For kit 1 and kit 2, two one-port standards are considered, including a 50 Ω match and an open device. None of these devices is part of the calibration devices.

Analyzing the differences between the measurement results and reference values acquired for the coaxial and WR5 bands, it seems that substrate aging may have a considerable impact on the transmission parameter magnitude. As the substrate conductivity properties seem susceptible to the ageing effect, they appear inversely proportional to frequency. This is evident from the improving agreement for the transmission parameter magnitude results observed for the upper half of the WR5 band and, subsequently, higher frequency bands. Several participating labs (among them PTB and FBH) observed these issues with the measurement repeatability and stability over longer periods of time, especially when analyzing the real part of the propagation constant extracted from the test structures. In an attempt to quantify the uncertainties associated with the effects observed, PTB determined the measurement repeatability from four repeat measurements of the entire kit 1 set of calibration standards and verification devices on two consecutive days. Consequently, for most measurands, repeatability formed the most significant component in the PTB uncertainty budget. More details on the composition of the PTB budget for various measurands are given in Section IV-E.

No noteworthy impact, i.e. results do not show discrepancies at transitions between frequency bands marked up to 330 GHz, is notable due to the differences in the used equipment in the used measurement systems, including different VNAs, probes, frequency extenders, and chucks as listed in Table IV.

As none of the other laboratories estimated the uncertainty contributions corresponding to their measurements, the combined uncertainty budget provided by PTB for kit 1 was analyzed further. As mentioned, the measurement repeatability was impaired by a lack of long-term stability in the test structures. It represents one of the most significant contributors to the PTB budget for most measurands. This is especially true for the magnitude of the reflection coefficient of the devices shown in Figs. 8 and 9. For the magnitude of the transmission coefficient of the 2-port devices shown in Figure 9, repeatability and crosstalk between the ports (defined as 'DUT uncertainty' in [15]) are the major contributors to an almost equal level, followed by the uncertainty contributions from the reference substrate calibration standards. This can explain the lack of agreement in the coaxial and WR5 band for the transmission parameter, as the reference value uncertainties do not take into account the repeatability uncertainty contributor. Only for the phase of the transmission coefficient of the 2-port devices of Figure 9, the uncertainty contributions from the calibration standards are typically the dominant component. Hence, it explains the good agreement for the transmission parameter phase for the kit-1 mismatched line.

Comparison of the uncertainty analysis corresponding to the PTB measurements and the simulation results highlights noteworthy differences, as evident from Figure 9(a) and Figure 9(c). Here, PTB uncertainty analysis accounts for more error sources as compared with the simulation results, which accounts only for the calibration standards and cross-talk uncertainty sources, as shown in Table VI. Furthermore, PTB and simulation uncertainty evaluations are performed entirely independently, i.e., calibration standard uncertainty corresponding to the simulations applies the maximal offset approach due to lack of information, which most likely results in overestimation of the uncertainty. This might be the reason for the larger uncertainties corresponding to the simulation results for the mismatched transmission line, as shown in Figure 9(c).

While no shifts are observed at the transition between WR2 and WR1.5 bands, a substantial shift is evident at the transition between WR1.5 and WR1 bands. Furthermore, WR1 results also show degradation in calibration accuracy, as evident from the Short and Open values exceeding 1 in linear magnitude. Here, the increased noisy behavior observed throughout the measurement results might suggest a degraded dynamic range or generation of higher-order modes, both error sources are not accounted for by the uncertainty analysis corresponding to the simulated reference values.

VI. Conclusion

This paper presents an on-wafer CPW measurement campaign ranging from 10 GHz to 1.1 THz. The measurement comparison is conducted using a dedicated reference substrate comprising two kits. The first kit (kit 1) is used for measurements from 10 GHz to 330 GHz, whereas the second kit (kit 2), focused on the 330 GHz to 1.1 THz range.

Measurement setups used by the participants include different vendor VNAs, frequency extender units, and probes, as shown in Table IV. Furthermore, probes also varied in pitch size between the laboratories.

Four laboratories participated in the measurement campaign up to 330 GHz for kit 1 and included measurements across the coaxial, WR5, and WR3 waveguide bands. The measurement results demonstrated excellent agreement despite the differences as mentioned earlier in the setups, and no abrupt shifts in results are evident when transitioning between frequency bands, see Figure 6. PTB estimated the combined uncertainty contribution corresponding to their measurements. The reference value and uncertainty estimates for the comparison devices primarily focused on accounting for calibration standards and probe crosstalk uncertainties. Both uncertainty estimates demonstrate similarity up to 330 GHz. The comparison results for kit 1 are in good agreement with the reference values and uncertainties.

Three laboratories participated in the measurements from 330 GHz up to 1.1 THz for kit 2, including measurements across WR2, WR1.5, and WR1 waveguide bands. The comparison results for kit 2 are in agreement with the estimated uncertainty as described earlier. However, the measurement results depict abrupt shifts when transitioning between the WR1.5 and WR1 frequency bands shown

in Figure 6. The calibration accuracy seems to degrade between 750 GHz and 1.1 THz range, as the reflection coefficient magnitude result for high reflect open device exceeds 1. Many possible reasons can cause this discrepancy, e.g. calibration standards and probe errors.

The agreement in reflection coefficient measurements of a one-port matched device is better than 0.08 in linear magnitude up to 330 GHz for kit 1 and 0.08 up to 1.1 THz for kit 2. The differences are well within the estimated uncertainties.

For highly reflective open devices, the difference in the reflection coefficient parameter is smaller than 0.1 for kit 1 and smaller than 0.18 for kit 2. Also, the differences between the mismatched devices are within the estimated uncertainties.

For two-port attenuator and mismatched transmission line devices, the transmission parameter S_{21} is compared.

The differences in the attenuator S_{21} magnitude with a nominal attenuation between 10 and 20 dB are smaller than 1.5 dB for kit 1 and smaller than 2 dB for kit 2. The results of the mismatched transmission line S_{21} magnitude are within 2 dB for both kits. For both two-port devices, the results agree reasonably well with the reference value uncertainties.

The S_{21} phase results for the mismatch transmission line show good agreement and are within reference value uncertainty up to 330 GHz. In the 330 GHz - 1.1 THz frequency range, it was not possible to compare the measurement values with reference values as the measurements were acquired at the different reference plane positions.

The design of the reference substrate on a semi-insulating high resistivity (>5000 Ω/cm) silicon (Si) wafer has proven to be suitable for designing high-accuracy reference substrates up to 750 GHz. At frequencies higher than 750 GHz, the calibration accuracy shows degradation and needs further investigation.

Furthermore, the use of EM simulations to acquire reference values for the comparison devices has proven highly promising. Where state-of-the-art simulation tools, such as CST Studio Suite®, can accurately model 3D structures, they are susceptible if inaccurate material characteristics are used, as evident from transmission parameter magnitude comparison results. Here, the material characteristics, frequency response, and its accuracy are critical elements for EM simulation tools to realize accurate results for frequencies exceeding 1 THz.

Finally, the interlaboratory comparison aimed at demonstrating the measurement accuracy of S-parameter systems up to 1.1 THz by using several verification devices with different properties, such as an attenuator and a mismatched transmission line. This allowed a detailed investigation into the sensitivity of the various error sources and the calibrated S-parameters. However, application-based sensitivity analysis between systems error sources and typical industrial measurement parameters of interest, i.e. transistor small signal equivalent circuit and model parameters such as f_{max} and noise figure, is not performed and will be considered in future work.

REFERENCES

[1] R. Singh, W. Cao, I. Al-Naib, L. Cong, W. Withayachumnankul, and W. Zhang, "Ultrasensitive terahertz sensing with high-q fano resonances in metasurfaces," *Applied Physics Letters*, vol. 105, Oct. 2014.

[2] P. Hillger, J. Grzyb, R. Jain, and U. R. Pfeiffer, "Terahertz imaging and sensing applications with silicon-based technologies," *IEEE Transactions on Terahertz Science and Technology*, vol. 9, pp. 1–19, Jan. 2019.

[3] K. B. Cooper, R. J. Dengler, N. Llombart, B. Thomas, G. Chattopadhyay, and P. H. Siegel, "Thz imaging radar for standoff personnel screening," *IEEE Transactions on Terahertz Science and Technology*, vol. 1, pp. 169–182, Sep. 2011.

[4] H. Tataria, M. Shafi, A. F. Molisch, M. Dohler, H. Sjöland, and F. Tufvesson, "6g wireless systems: Vision, requirements, challenges, insights, and opportunities," *Proceedings of the IEEE*, vol. 109, pp. 1166–1199, Jul. 2021.

[5] M. Urteaga, Z. Griffith, M. Seo, J. Hacker, and M. J. W. Rodwell, "Inp hbt technologies for thz integrated circuits," *Proceedings of the IEEE*, vol. 105, pp. 1051–1067, Jun. 2017.

[6] X. Mei, W. Yoshida, M. Lange, J. Lee, J. Zhou, P.-H. Liu, K. Leong, A. Zamora, J. Padilla, S. Sarkozy, R. Lai, and W. R. Deal, "First demonstration of amplification at 1 thz using 25-nm inp high electron mobility transistor process," *IEEE Electron Device Letters*, vol. 36, pp. 327–329, Apr. 2015.

[7] M. Horibe, "Improvement of measurement uncertainty of thz waveguide vector network analyzers," in *2021 96th ARFTG Microwave Measurement Conference (ARFTG)*. IEEE, Jan. 2021, pp. 1–4.

[8] L. Xie, M. F. Bauwens, S. Nadri, A. Arsenovic, M. E. Cyberey, A. W. Lichtenberger, N. S. Barker, and R. M. Weikle, "Electronic calibration for submillimeter-wave on-wafer scattering parameter measurements using schottky diodes," *IEEE Transactions on Terahertz Science and Technology*, vol. 10, pp. 583–592, Nov. 2020.

[9] M. F. Bauwens, N. Alijabbari, A. W. Lichtenberger, N. S. Barker, and R. M. Weikle, "A 1.1 thz micromachined on-wafer probe," in *2014 IEEE MTT-S International Microwave Symposium (IMS2014)*. IEEE, Jun. 2014, pp. 1–4.

[10] BIPM, "Bipm kcdb," Aug. 2023. [Online]. Available: https://www.bipm.org/kcdb/

[11] D. F. Williams, A. C. Young, and M. Urteaga, "A prescription for sub-millimeter-wave transistor characterization," *IEEE Transactions on Terahertz Science and Technology*, vol. 3, pp. 433–439, Jul. 2013.

[12] J. Cabello-Sanchez, H. Rodilla, V. Drakinskiy, and J. Stake, "Multiline trl calibration standards for s-parameter measurement of planar goubau lines from 0.75 thz to 1.1 thz," in *2018 IEEE/MTT-S International Microwave Symposium - IMS*. IEEE, Jun. 2018, pp. 879–882.

[13] J. Cabello-Sánchez, V. Drakinskiy, J. Stake, and H. Rodilla, "A corrugated planar-goubau-line termination for terahertz waves," *IEEE Microwave and Wireless Technology Letters*, vol. 33, pp. 643–646, Jun. 2023.

[14] J. Cheron, R. D. Jones, D. F. Williams, M. E. Urteaga, B. T. Bosworth, N. R. Jungwirth, J. A. Jargon, B. F. Jamroz, C. J. Long, N. D. Orloff, A. D. Feldman, and P. H. Aaen, "A 0.1 ghz to 1.1 thz inverted grounded-cpw mtrl calibration kit characterization in an inp hbt process," in *2024 IEEE Wireless and Microwave Technology Conference (WAMICON)*. IEEE, Apr. 2024, pp. 1–4.

[15] U. Arz, K. Kuhlmann, T. Dziomba, G. Hechtfischer, G. N. Phung, F. J. Schmückle, and W. Heinrich, "Traceable coplanar waveguide calibrations on fused silica substrates up to 110 ghz," *IEEE Transactions on Microwave Theory and Techniques*, vol. 67, pp. 2423–2432, 2019.

[16] U. Arz, S. Zinal, T. Probst, G. Hechtfischer, F.-J. Schmuckle, and W. Heinrich, "Establishing traceability for on-wafer s-parameter measurements of membrane technology devices up to 110 ghz," in *2017 90th ARFTG Microwave Measurement Symposium (ARFTG)*. IEEE, Nov. 2017.

[17] M. Horibe, "Measurement uncertainty model for vector network analyzers with frequency extension modules at terahertz frequencies," *IEEE Transactions on Instrumentation and Measurement*, vol. 66, pp. 1605–1612, Jun. 2017.

[18] A. Bystrov, Y. Wang, and P. Gardner, "Analysis of vector network analyzer thermal drift error," *Metrology*, vol. 2, pp. 150–160, Mar. 2022.

[19] Y. Zantah, A. Batra, A. Prokscha, F. Sheikh, M. Haidar, N. Zarifeh, A. A. Abbas, and T. Kaiser, "Experimental analysis of vna-based measurement errors in mobile thz applications," in *2023 Sixth International Workshop on Mobile Terahertz Systems (IWMTS)*. IEEE, Jul. 2023, pp. 1–5.

[20] R. D. Jones, J. Cheron, B. F. Jamroz, W. R. Deal, M. Urteaga, D. F. Williams, A. D. Feldman, P. H. Aaen, C. J. Long, and N. D. Orloff, "On-wafer capacitor characterization including uncertainty estimates up to 1.0 thz," *IEEE Transactions on Terahertz Science and Technology*, vol. 14, pp. 734–744, Sep. 2024.

[21] T. Probst, R. Doerner, M. Ohlrogge, R. Lozar, and U. Arz, "110 ghz on-wafer measurement comparison on alumina substrate," in *2017 90th ARFTG Microwave Measurement Symposium (ARFTG)*. IEEE, Nov. 2017.

[22] R. G. Clarke, C. Li, and N. M. Ridler, "An intra-laboratory investigation of on-wafer measurement reproducibility at millimeter-wave frequencies," in *2017 90th ARFTG Microwave Measurement Symposium (ARFTG)*. IEEE, Nov. 2017.

[23] A. Rumiantsev, R. Doerner, J. Martens, and S. Reyes, "Inter-laboratory comparison of on-wafer broadband 70khz-220ghz single-sweep measurements," in *2021 51st European Microwave Conference (EuMC)*. IEEE, Apr. 2022, pp. 425–428.

[24] R. D. Jones, J. Cheron, B. T. Bosworth, B. F. Jamroz, D. F. Williams, M. E. Urteaga, A. D. Feldman, and P. H. Aaen, "Microstrip and grounded cpw calibration kit comparison for on-wafer transistor characterization from 220 ghz to 325 ghz," in *2023 IEEE BiCMOS and Compound Semiconductor Integrated Circuits and Technology Symposium (BCICTS)*. IEEE, Oct. 2023, pp. 124–127.

[25] T. Karpisz, J. Pawlik, J. Hoffmann, S. R. Evans, C. J. Long, N. D. Orloff, J. C. Booth, and A. Stelson, "On-wafer calibration comparisons of multiline trl with platinum and gold conductors," in *2024 IEEE/MTT-S International Microwave Symposium - IMS 2024*. IEEE, Jun. 2024, pp. 1020–1023.

[26] X. Shang, N. Ridler, U. Arz, G. N. Phung, I. Roch-Jeune, G. Ducournau, K. Haddadi, T. Flisgen, R. Doerner, D. Allal, D. Jayasankar, J. Stake, R. Schmidt, G. Fisher, and F. Mubarak, "Interlaboratory investigation of on-wafer s-parameter measurements from 110 ghz to 1.1 thz," in *2023 53rd European Microwave Conference (EuMC)*. IEEE, Sep. 2023, pp. 624–627.

[27] F. Mubarak, V. Mascolo, G. Rietveld, M. Spirito, K. Daffe, and K. Haddadi, "Parameterization models for traceable characterization of planar cpw sol calibration standards," in *2018 Conference on Precision Electromagnetic Measurements (CPEM 2018)*. IEEE, Jul. 2018.

[28] L. Sevgi, "Electromagnetic modeling and simulation: Challenges in validation, verification, and calibration," *IEEE Transactions on Electromagnetic Compatibility*, vol. 56, pp. 750–758, Aug. 2014.

[29] R. Kacker, R. Datla, and A. Parr, "Statistical interpretation of key comparison reference value and degrees of equivalence," *Journal of Research of the National Institute of Standards and Technology*, vol. 108, p. 439, Nov. 2003.

[30] R. B. Marks, "A multiline method of network analyzer calibration," *IEEE Transactions on Microwave Theory and Techniques*, vol. 39, pp. 1205–1215, 1991.

[31] R. G. Clarke, X. Shang, N. M. Ridler, R. Lozar, T. Probst, and U. Arz, "An interlaboratory study of the reproducibility of on-wafer s-parameter measurements from 140 ghz to 220 ghz," in *2020 94th ARFTG Microwave Measurement Symposium (ARFTG)*. IEEE, Jan. 2020, pp. 1–4.

[32] D. DeGroot, J. Jargon, and R. Marks, "Multiline trl revealed," in *60th ARFTG Conference Digest, Fall 2002*. IEEE, pp. 131–155.

[33] K. Silvonen, "A general approach to network analyzer calibration," *IEEE Transactions on Microwave Theory and Techniques*, vol. 40, pp. 754–759, Apr. 1992.

[34] D. F. Williams, C. M. Wang, and U. Arz, "An optimal multiline trl calibration algorithm," in *Microwave Symposium Digest, 2003 IEEE MTT-S International*, vol. 3, 2003, pp. 1819–1822.

[35] R. Schmidt, S. Clochiatti, E. Mutlu, N. Weimann, A. Ferrero, M. Dieudonne, and D. M. M.-P. Schreurs, "Compensating probe misplacements in on-wafer s-parameters measurements," *IEEE Transactions on Microwave Theory and Techniques*, pp. 1–11, 2022.

[36] G. N. Phung, U. Arz, K. Kuhlmann, R. Doerner, and W. Heinrich, "Improved modeling of radiation effects in coplanar waveguides with finite ground width," in *2020 50th European Microwave Conference (EuMC)*. IEEE, Jan. 2021, pp. 404–407.

[37] G. N. Phung and U. Arz, "Anomalies in multiline-trl-corrected measurements of short cpw lines," in *2021 96th ARFTG Microwave Measurement Conference (ARFTG)*. IEEE, Jan. 2021, pp. 1–4.

[38] ——, "On the influence of thru- and line-length-related effects in cpw- based multiline trl calibrations," in *2021 97th ARFTG Microwave Measurement Conference (ARFTG)*. IEEE, Jun. 2021, pp. 1–4.

[39] "Ind02 'planarcal' best practice guide for planar s-parameter measurements using vector network analysers." [Online]. Available: https://planarcal.ptb.de/14ind02home.html,

[40] E. A. of National Metrology Institutes, "Guidelines on the evaluation of vector network analyzers (vna) - version 3.0," 2018.

Faisal Ali Mubarak received an M.Sc. degree in electrical engineering in 2009 and a Ph.D. in microwave measurements in 2025 from Delft University of Technology, The Netherlands. In 2009, he joined the VSL, the national measurement institute of the Netherlands, where he is presently a Principal Scientist on RF & MW measurements. His research interests include developing RF measurement systems and techniques up to millimetre-wave frequencies. In 2017, he was one of the co-founders of Vertigo Technologies, Delft, a company developing innovative measurement techniques and instruments.

Mr Mubarak is a member of the International Consultative Committee for Electricity and Magnetism Working Group on Radiofrequency Quantities and the European Association of National Metrology Institutes technical sub-committee on Radio frequencies and Microwaves (WG-RF). He is also a serving member of the European Metrology Network on Quantum Technologies (EMNQ) and the IEEE MTT-11 Technical Committee.

Gia Ngoc Phung received the Dipl.-Ing. and Ph.D. degrees from the Technical University of Berlin, Berlin, Germany, in 2012 and 2021, respectively. From 2013 to 2015, she worked at Biotronik SE & Co. KG, Berlin, where she worked on electromagnetic simulation of cardiac devices. From 2015 to 2019, she was with the Ferdinand-Braun-Institut (FBH), Berlin, where she worked on her Ph.D. thesis, mainly in the field of modelling and characterisation of on-wafer measurements and microwave packaging at millimeter-wave frequencies. Since October 2019, she has been working at the Physikalisch-Technische Bundesanstalt, Braunschweig, Germany. Her main research interests are on-wafer, dielectric material and RF power metrology. She was awarded the Young Scientist Award of the Kleinheubach Conference 2021 and was co-recipient of the European Microwave Prize 2011. She is currently leading the European Partnership on Metrology (EPM) project OnMicro 23IND10 as a project coordinator.

Uwe Arz received the Dipl.-Ing. degree in electrical engineering and the Ph.D. degree (summa cum laude) from the University of Hannover, Hannover, Germany, in 1994 and 2001, respectively. In 2001, he served as a Post-Doctoral Research Associate with the National Institute of Standards and Technology, Boulder, CO, USA. In 2002, he joined the Physikalisch-Technische Bundesanstalt (PTB), Brunswick, Germany, where he develops metrology for on-wafer measurements. From 2015 to 2018, he led the European EMPIR Project PlanarCal as a Coordinator. He is currently the Head of the Working Group On-Wafer Scattering Parameter Measurements at PTB. He has authored and coauthored more than 100 publications in the fields of on-wafer S-parameter measurements, broadband characterization of high-speed interconnects, high-impedance probing, network analyzer calibration, and dielectric material measurements. He is the recipient of the first ARFTG Microwave Measurement Student Fellowship Award in 1999 and the 2003 AHMT Measurement Award presented by the Association of German University Professors for Measurement Science. He received three ARFTG Best Poster and two ARFTG Best Paper Awards, and was a co-recipient of the 2011 European Microwave Prize. In January 2023 Dr. Arz was honored as an ARFTG Life Member.

Guillaume Ducournau is with the Institute of Electronics, Microelectronics and Nanotechnology (IEMN), UMR-CNRS 8520, University of Lille, Villeneuve d'Ascq, France, since 2007. He is the Leader of the THz wireless communications activity with IEMN using optoelectronic THz photomixers, electronic receivers, THz instrumentation, and millimeter-wave (mm-wave) characterization. He worked on several European projects: STREP ROOTHz 2010-2013, ThoR H2020, GRAPH-X, TIMES (6G SNS) as well as the Marie-Skłodowska Curie TERAOPTICS network. At national level he was the Coordinator of the COM'TONIQ Project from 2014 to 2017 funded by ANR (INFRA 2013) dedicated to THz communications in the 300 GHz band, the ANR/DFG TERASONIC project for the use of THz photonics technologies and electrical solid-state technologies for THz communications and SPATIOTERA for spatially-distributed photomixers. He received the 2020 ISAP BEST PAPER award. He is involved in national France 2030 programs gathering several French laboratories under the 'PEPR' programs funded by the ANR (Agence Nationale de la Recherche). In this framework, the FUNTERA project (6 partners) is investigating THz converters, while the SYSTERA project (12 partners) is dedicated to beyond 90 GHz systems for future networks. He also participates to the ST-IEMN common laboratory, and more specifically involved in the mm-wave technologies characterization part. He has authored or co-authored more than 180 publications in peer-reviewed international journals or peer-reviewed conferences proceedings and holds 1 patent.

Thomas Flisgen received the Diploma degree in electrical engineering/telecommunications engineering from the Hochschule Niederrhein, Krefeld, Germany, in 2007, the Master degree in 2009 and the PhD in computational engineering in 2015, both, from the University of Rostock, Rostock, Germany. From 2017 to 2018 he was scientist for wakefields and impedances at Helmholtz-Zentrum Berlin. From 2018 to 2024 he was head of the electromagnetic field simulation group at Ferdinand-Braun-Institut gGmbH, Leibniz-Institut für Höchstfrequenztechnik. Since autumn 2024 he is full professor at the Brandenburg University of Technology and holds the Chair of Electromagnetic Field Theory.

Ralf Doerner received the Dipl. Ing. degree in communications engineering from the Technische Universität Ilmenau, Ilmenau, Germany, in 1990.

Since 1989, he has been working on microwave measuring techniques. In 1992, he joined the Ferdinand-Braun-Institut, Leibniz-Institut für Höchstfrequenztechnik, Berlin, Germany. His current research is focused on calibration problems in on-wafer millimeter-wave and sub-millimeter-wave measurements of active and passive devices and circuits. Further research activities include nonlinear characterization of microwave power transistors and noise characterization and modeling of microwave devices.

Djamel Allal received the Ing. degree in electronics from the University of Science and Technology Houari Boumediene, Algiers, Algeria, in 1991, and the Ph.D. degree in electronics from the University of Lille, Villeneuve d'Ascq, France, in 1997. He joined the Laboratoire National de Métrologie et d'Essais (LNE), Trappes, France, in 2001, where he has been working in research activities in the field of RF and microwave metrology. His current activities include the development of measurement standards in power and in coaxial and on-wafer S parameters, the development of measurement methods for microwave and terahertz electromagnetic materials characterization, and the development of measurement capabilities of electromagnetic field and specific absorption rate.

Divya Jayasankar was born in India in 1994. She received her bachelor's degree in electronics and communication engineering in 2015. Followed by a master's degree in wireless, photonics and space engineering and a PhD degree in terahertz electronics from Chalmers University of Technology, Sweden, in 2019 and 2024, respectively. From 2015 to 2017, she worked as a research assistant at Raman Research Institute in India. Since 2025, she has been a postdoctoral researcher at the German Aerospace Centre (DLR). During her PhD, she worked as a visiting PhD student at DLR in 2021, the University of Warwick in 2022, and Virginia Diodes Inc. (VDI) in 2023. Her research interests include the development of THz front-end receivers for space/airborne missions and THz metrology. D. Jayasankar received the Ericsson Research Foundation award, the European Microwave Association (EuMA) internship award, the IEEE-MTTs graduate fellowship, and the Roger Pollard fellowship for microwave measurements by ARFTG. In 2022, she also won second place in the best student paper competition at the ISSTT conference in Baeza, Spain.

Jan Stake (S'95–M'00–SM'06) was born in Uddevalla, Sweden, in 1971. He received an M.Sc. in electrical engineering and a Ph.D. in microwave electronics from Chalmers University of Technology in Gothenburg, Sweden, in 1994 and 1999, respectively.

In 1997, he was a Research Assistant at the University of Virginia, Charlottesville, VA, USA. From 1999 to 2001, he was a Research Fellow with the Millimetre Wave Group at the Rutherford Appleton Laboratory, Didcot, UK. He then joined Saab Combitech Systems AB, Gothenburg, Sweden, as a Senior RF/microwave Engineer until 2003. From 2000 to 2006, he held different academic positions with the Chalmers University of Technology, and from 2003 to 2006, he was also the Head of the Nanofabrication Laboratory, Department of Microtechnology and Nanoscience (MC2). In 2006, he was appointed Professor and the Head of the Terahertz and Millimetre Wave Laboratory at the Chalmers University of Technology. He was a Visiting Professor with the Submillimeter Wave Advanced Technology (SWAT) Group at Caltech/JPL, Pasadena, CA, USA, in 2007 and at TU Delft, the Netherlands, in 2020. He received an appointment as a visiting research fellow at the National Physical Laboratory, UK, in the year 2023. He is also the co-founder of Wasa Millimeter Wave AB, Gothenburg, Sweden. His research interests include high-frequency semiconductor devices, terahertz electronics, submillimeter wave measurement techniques, and terahertz systems.

Prof. Stake served as the Editor-in-Chief for the IEEE Transactions on Terahertz Science and Technology between 2016 and 2018 and as Topical Editor between 2012 and 2015. From 2019 to 2021, he was chairperson of the IEEE THz Science and Technology Best Paper Award committee. He is an elected member of the International Society of Infrared, Millimeter and Terahertz Waves (IRMMW-THz) board.

Nick M. Ridler received the B.Sc. degree from King's College London, U.K., in 1981. He is currently Head of Science for Electromagnetic and Electrochemical Technologies at the UK's National Physical Laboratory (NPL), U.K. He is also an Honorary Professor at the Universities of Glasgow and Liverpool, U.K., and a Visiting Professor at the Universities of Kent, Leeds, and Strathclyde, U.K. He is Non-Executive Director of LA Techniques Ltd and a member of the Board of Directors of the European Microwave Association (EuMA). He has more than 40 years' experience working in industrial, government and academic research establishments. His current interests include making accurate electromagnetic measurements at high frequencies (i.e., from approximately 1 kHz to 1 THz). He is an NPL Fellow, and Fellow of the Institute of Electrical and Electronics Engineers (IEEE), the Institution of Engineering and Technology (IET) and the Institute of Physics (IOP). He was General Chair of the 2021 European Microwave Week.

Robin Schmidt graduated in 2018 as an Electrical Engineer from l'École Supérieur d'Électricité (Supélec). Now employed as a researcher by Keysight Technology Belgium and pursuing the Ph.D. at University of Leuven (KU Leuven), his focus is the development of calibration for on-wafer S-parameters measurements in mm and sub-mm-wave frequency.

Gavin Fisher is applications specialist for the Centre of Expertise at FormFactor working on RF application layers for the systems group providing application support and technical services to FormFactor's customers as well as evaluating and developing new product. With two decades of experience working with Formfactor / Cascade probe systems and probes and a broad spectrum of applications such as high-frequency measurement, calibration and power device measurement, he educates and trains customers on best practices to achieve accurate measurement results. He has made several presentations at European Microwave Week, International Microwave Symposium, MOS-AK workshops, and Agilent/Keysight seminars. He holds an upper-second degree from Brunel University in Mechanical Engineering with electronic systems.

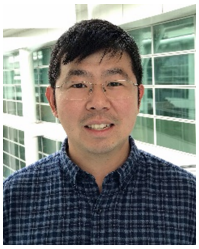

Xiaobang Shang received the B.Eng. degree (First Class) in electronics and communication engineering in 2008 and the Ph.D. degree in microwave engineering in 2011 from the University of Birmingham, U.K. He became a Senior Scientist at the National Physical Laboratory (NPL), Teddington, U.K., in 2017 and was promoted to Principal Scientist in 2023. He has authored or coauthored more than 120 scientific articles on microwave measurements and microwave circuits.

Dr. Shang is a member of IEEE MTT-S Technical Committee (TC)-3 and TC-21 and was an Associate Editor for the IEEE Microwave and Wireless Technology Letters (2020-2024). He was a recipient of several prestigious awards including the IEEE MTT-S Outstanding Young Engineer Award in 2025, the Roberto Sorrentino Prize in 2022, the IEEE Tatsuo Itoh Award in 2017, and the ARFTG Microwave Measurement Student Fellowship Award in 2009.